Trailing Edge Noise Prediction

Large-Eddy Simulation of Wall Bounded Shear Flow Using the Nonlinear Disturbance Equations

Final Report
Contract No. N-00014-99-0290

26 September 2000

Submitted to:

L. Patrick Purtell
Office of Naval Research
800 North Quincy St.
Arlington, VA 22217-5660

Prepared by:

T. S. Chyczewski

Applied Research Laboratory
The Pennsylvania State University
P.O. Box 30
State College, PA 16803

20001003 083

SUMMARY

The potential benefits of using the Nonlinear Disturbance (NLD) equations, which govern flow variable fluctuations about an estimated mean, for the large-eddy simulation (LES) of wall bounded shear flows are investigated under this grant. In addition to verifying the suitability of the NLD equations for wall bounded flows, we build upon its advantages by introducing a new wall model that is easily and efficiently implemented within the NLD equation framework. The model implementation consists of defining a near wall region in which a modified linear set of equations are solved. The linear equation set allows disturbances to pass through and interact with the wall without altering the estimated mean. The streamwise and spanwise grid resolution of this near wall region can therefore be significantly relaxed while maintaining reasonable mean quantities such as skin friction. Comparisons of predicted turbulence intensity profiles and wall pressure spectra to experimental data for a fully developed turbulent flat plate boundary layer are used to verify the suitability of the NLD equations for wall bounded flows. Preliminary results of a turbulent channel flow simulation are also presented to assess the new wall model.

1. INTRODUCTION

The NLD equations were introduced as an alternative form of the Navier Stokes equations for computational aeroacoustic (CAA) problems by Morris *et al.*[1]. Among other things, such problems require that small amplitude, high frequency acoustic waves be accurately simulated in the presence of much larger, low frequency flow variations.

The NLD equation approach addresses this requirement in two ways. First, these equations solve for flow variable fluctuations rather than the entire variable. Small amplitude fluctuations are therefore better represented with the available finite computer precision. Second, the implementation of far field boundary conditions is improved with the NLD equations approach since these conditions are oftentimes formulated in terms of equations linearized about a mean flow (e.g. [2],[3]). Using the estimated mean to close the far field boundary condition equations leads to improved performance of these equations over other methods of specifying a mean, such as local space or time averaging. Poor implementations of far field boundary conditions can lead to significantly contaminated acoustic solutions and excessive integration time required to propagate initial transients out of the computational domain.

The NLD equations approach has been applied to a number of problems including jet flow and noise radiation[1], ship airwake simulations[4] and aircraft engine liner simulations[5]. Under this grant, we investigated the suitability of this approach to wall bounded shear flows with the ultimate goal of applying it to CAA problems dependent on boundary layer turbulence, such as trailing edge noise or flap side edge noise. In addition, we looked to build upon the advantages of this approach by developing a wall model that is easily implemented within the framework of the NLD equations.

Wall models attempt to reduce the computational expense of accurate wall bounded shear flow simulations by modeling rather than simulating the very small relevant turbulent scales of the inner regions of a boundary layer. Eliminating the necessity of resolving these scales significantly relaxes the grid spacing requirements which in turn reduces the required number of grid points and allows for much larger time steps.

Wall models have typically been implemented in one of three ways. In the first, the computational domain begins above the wall usually in the log-law region of the boundary layer and a wall stress boundary condition is specified[6][7]. In the second, the computational domain is decomposed into two regions; an outer region where an LES is performed and an inner region where the boundary layer or Reynolds Averaged Navier Stokes (RANS) equations are solved[8]. The third is similar to the second except that, rather than specifying two distinct regions, the eddy viscosity is allowed to smoothly transition from a RANS type to an LES type depending on the grid resolution[9][10].

The wall model implemented here is similar to third type listed above in that the equations transition from one type near the wall to another away from the wall. However, instead of transitioning from LES to RANS, we transition from LES to a linear perturbation equation set by damping out selected terms of the NLD equations. The advantage is that the implementation is relatively simple and computationally efficient. A potential drawback of this approach is that its performance may depend on the fidelity of the estimated mean flow.

The remainder of the report is organized as follows: Section 2 presents the NLD equations and discusses the potential impacts of the estimated mean. In section 3 the subgrid scale (SGS) turbulence model is described as well as the new wall model. The numerical algorithm and parallel implementation are discussed in section 4. In section 5 results of turbulent channel flow and flat plate boundary layer simulations are presented. Finally, some conclusions are drawn in section 6.

2. GOVERNING EQUATIONS

2.1 NLD Equations

A filtered version of the NLD equations are solved. The starting point for the development of these equations is the selection of a filtering procedure for the compressible Navier Stokes equations. Rather than using Favre averaged variables, we decompose the unaveraged variables into grid resolved and subgrid scale components. Upon substituting this decomposition into the Navier Stokes equations and filtering, the extra subgrid scale terms due to compressibility are subsequently discarded since we are interested only in low Mach number compressible flow.

One arrives at the filtered NLD equations by decomposing the resolved flow variables of the filtered Navier Stokes equations into two components, substituting them into the filtered Navier Stokes equations and rearranging terms. The two components of each variable are chosen to be (1) an *a priori* prediction of the mean quantity (referred to here as the estimated mean) and (2) the grid resolved part of the fluctuation away from the estimated mean:

$$q^r = \bar{q} + q'^r \tag{1}$$

where the superscript 'r' denotes a filtered quantity, an overbar denotes the estimated mean component and the prime denotes a fluctuation quantity. The variables that are decomposed in this manner are the density, ρ, the velocity vector, u_j, the pressure, p, and the total energy, e.

Upon substituting this decomposition into the Navier Stokes equations, the NLD equations can be rearranged into a conserved variable time derivative term, linear and nonlinear inviscid flux terms, SGS stress terms, source terms and, except for the continuity equation, viscous terms. The viscous term for the energy equation also includes a heat conduction term. The source terms consist of all of the terms that are independent of the fluctuating quantities and can be shown to be equal to the Reynolds stresses associated with the estimated mean.

The equations are given below with all of the SGS stress terms included. Each equation has six terms in curly brackets corresponding to the terms listed above (except for continuity which does not have a viscous term). The variables have been nondimensionalized as follows:

$$\rho = \frac{\rho^*}{\rho_\infty}, \quad u_j = \frac{u_j^*}{c_\infty}, \quad p = \frac{p^*}{\rho_\infty c_\infty^2}$$

$$e = \frac{e^*}{\rho_\infty c_\infty^2}, \quad x_j = \frac{x_j^*}{L}$$

(2)

where an asterisk denotes a dimensional quantity, c is the sound speed, L is a reference length and the subscript ∞ denotes the dimensional freestream value.

Continuity:

$$\{\rho^{r}_{,t}\} + \{(\bar{\rho}u_j^{\prime r} + \rho^{\prime\prime r}\bar{u}_j)_{,j}\} + \{(\rho^{\prime\prime}u_j^{\prime\prime})_{,j}\} =$$

$$-\{[(\rho u_j)^r - \rho^r u_j^r]_{,j}\} - \{\bar{\rho}_{,t} + (\bar{\rho}\bar{u}_j)_{,j}\}$$

(3)

Momentum:

$$\{(\bar{\rho}u_i^{\prime r} + \rho^{\prime\prime r}\bar{u}_i + \rho^{\prime\prime}u_i^{\prime\prime r})_{,t}\} +$$

$$\{(\bar{\rho}\bar{u}_i u_j^{\prime r} + \bar{\rho}u_i^{\prime\prime r}\bar{u}_j + \rho^{\prime\prime r}\bar{u}_i\bar{u}_j + \delta_{ij}p)_{,j}\} +$$

$$\{(\bar{\rho}u_i^{\prime r}u_j^{\prime r} + \rho^{\prime\prime r}\bar{u}_i u_j^{\prime\prime} + \rho^{\prime\prime}u_i^{\prime\prime r}\bar{u}_j + \rho^{\prime\prime}u_i^{\prime\prime}u_j^{\prime\prime r})_{,j}\} =$$

$$-\{[(\rho u_i u_j)^r - \rho^r u_i^r u_j^r]_{,j} + [(\rho u_i)^r - \rho^r u_i^r]_{,t}\}$$

$$-\{(\bar{\rho}\bar{u}_i)_{,t} + (\bar{\rho}\bar{u}_i\bar{u}_j + \delta_{ij}\bar{p} - \bar{\tau}_{ij})_{,j}\} + \{(\tau'_{ij})_{,j}\}$$

(4)

Energy:

$$\{e^{\prime r}_{,t}\} + \{[\bar{u}_j(e^{\prime r} + p^{\prime r}) + u_j^{\prime r}(\bar{e} + \bar{p})]_{,j}\} +$$

$$\{[u_j^{\prime r}(e^{\prime r} + p^{\prime r})]_{,j}\} =$$

$$-\{[(u_j(e+p))^r - u_j^r(e+p)^r]_{,j} - [(u_i\tau_{ij})^r - u_i^r\tau_{ij}^r]_{,j}\}$$

$$-\{\bar{e}_{,t} + [\bar{u}_j(\bar{e} + \bar{p}) - (\bar{u}_i\bar{\tau}_{ij} - \bar{q}_j)]_{,j}\} +$$

$$\{[(\bar{u}_i\tau_{ij}^{\prime r} + u_i^{\prime\prime r}\bar{\tau}_{ij} + u_i^{\prime\prime}\tau_{ij}^{\prime\prime r}) - q_j^{\prime r}]_{,j}\}$$

(5)

where the viscous stress tensor and the heat flux are given by

$$\tau_{ij} = \frac{1}{Re}\left(u_{i,j} + u_{j,i} - \frac{2}{3}u_{k,k}\delta_{ij}\right)$$

(6)

$$q_j = -\frac{T_{,j}}{Re Pr(\gamma - 1)}$$

(7)

γ is the ratio of specific heats and Re and Pr are the Reynolds and Prandtl numbers, respectively, given by

$$Re = \frac{\rho_\infty c_\infty L}{\mu_\infty}, \quad Pr = \frac{\mu C_p}{k}$$

(8)

3

2.2 Estimated Mean

In the present study a Reynolds Averaged Navier Stokes (RANS) solver (with a q-ω turbulence model) is used to supply the estimated mean. Since, so far in the development of the NLD equations, we have not considered discarding any terms, the fluctuating variables will in general develop a mean component that when added to the estimated mean will provide the mean quantity that would be predicted by the traditional form of the Navier Stokes equations. In this respect, the solution is independent of the estimated mean. However, the fidelity of the estimated mean can impact the NLD equations solution in ways that could reduce or eliminate the advantages of using the NLD approach.

One of the advantages of the NLD equation approach, when one considers acoustic predictions, is that the fluctuating component is stored separately from the estimated mean which consequently leads to a reduction in the impact of computer roundoff errors. If the estimated mean differs significantly from the mean that would be predicted from the traditional Navier Stokes equations then the 'fluctuating' component would develop a mean component and the roundoff error reduction will not be realized. For most aeroacoustic problems, it is relatively easy to predict accurate mean flows in the acoustic near and far fields. If one considers the density, which is typically used as an acoustic variable, predicting the mean value is trivial for the low Mach number flows of interest here.

Another advantage of the NLD equation approach that can be impacted by a poor estimation of the mean flow is the simplified implementation of boundary conditions. In the current work, for the flat plate boundary layer case, the estimated mean is used both for the radiation condition opposite the wall and for the inflow recycling condition used in the streamwise direction (these boundary conditions will be discussed further in section 2.3). A poorly estimated mean field can result in reflections at the radiation boundary and incorrect boundary layer growth rates due to the recycling condition. The final advantage that can be impacted by the estimated mean is the simplified wall model that is discussed in section 3.2

2.3 Boundary Conditions

Fully developed turbulence simulations of a channel flow and a flat plate boundary layer were performed. For the channel flow case, periodic conditions are used in both the spanwise and streamwise flow directions. At the walls a no slip, adiabatic condition is imposed.

The wall is treated in the same manner for the flat plate boundary layer case. Opposite the wall, the radiation boundary condition developed in Tam and Webb[2] is used. Spatial periodicity is used in the spanwise direction. The inflow condition is specified using the recycling boundary condition of Lund *et al.* [11] in which the flow variables are sampled at a downstream location, scaled based on mean local boundary layer quantities and reintroduced at the inflow. The estimated mean flow is used to scale the variables here. The buffer zone developed by Wasistho *et al.*[12] is used at the outflow. This zone is approximately six boundary layer thicknesses long with grid points stretched in the axial direction and starts more than one boundary layer thickness downstream of the location where the flow variables are sampled for the inflow condition.

3. MODELING

3.1 Subgrid Scale Stress Model

As mentioned in section 2.1, the SGS stress terms associated solely with compressibility are discarded. For the continuity equation, this leads to:

$$-[(\rho u_j)^r - \rho^r u_j^r]_{,j} = 0 \tag{9}$$

For the momentum equations, the compressible extension of the Smagorinsky model as outlined by Moin *et al.*[13] is used except we do not employ the dynamic procedure for specifying the model coefficients. It has the form:

$$-[(\rho u_i u_j)^r - \rho^r u_i^r u_j^r] = \left[\rho \upsilon_T \tau_{ij} - \frac{1}{3}q^2\delta_{ij}\right]_{,j} \tag{10}$$

$$[(\rho u_i)^r - \rho^r u^r]_{,t} = 0$$

where the second equation is associated with compressibility and

$$\upsilon_T = C_s \Delta^2 |S^r| Re$$
$$q^2 = 2C_I \rho \Delta^2 |S^r|^2 Re \tag{11}$$

with

$$|S^r| = \sqrt{2S_{ij}^r S_{ij}^r} \tag{12}$$

and

$$S_{ij}^r = \frac{1}{2}(u_{i,j}^r + u_{j,i}^r) \tag{13}$$

Δ is the filter width chosen here to be

$$\Delta = (\Delta x \Delta y \Delta z)^{1/3} \tag{14}$$

Finally, the energy equation SGS terms are modeled by:

$$-[(u_j(e+p))^r - u_j^r(e+p)^r]_{,j} = -q_{j,j}^{sgs} \tag{15}$$

$$[(u_i \tau_{ij})^r - u_i^r \tau_{ij}^r]_{,j} = 0$$

where

$$q_j^{sgs} = -\frac{1}{\gamma(\gamma-1)Pr_T Re}\rho \upsilon_T T_{,j} \tag{16}$$

Pr_T is the turbulent Prandtl number. Unlike [13], constant coefficients are used with the van Dreist near wall damping. We choose $C_S = 0.012$, $C_I = 0.0066$ and $Pr_T = 0.60$. The van Driest damping takes the form

$$C_S^{vd} = C_S \left(1 - \exp\left(-\frac{y^+}{A^+}\right)\right)^2 \tag{17}$$

where A^+ is set to 25.

3.2 Wall Model

Under this grant, potential additional advantages of using the NLD equations were investigated by developing a wall model that is easily implemented within the NLD equation framework and is computationally very efficient. The idea is to modify the equations in the near wall region so that the mean of each fluctuating variable is forced to be zero. This consequently forces the mean of the total variable to be equal to the estimated mean.

This is accomplished by damping out the nonlinear inviscid flux, SGS and source terms near the wall. Having eliminated these terms, we are left with the linear inviscid flux and the viscous terms. With the exception of the energy equation viscous term, the near wall equations are linear and as such cannot develop a mean quantity. The nonlinear term in the energy equation is not expected to be significant in the low Mach number flows of interest here but has been retained for computational convenience.

The model is implemented by defining a variable λ that varies from zero at the wall to unity at a specified location in the boundary layer. As implemented here, the location where λ equals unity is a function of y^+ as determined from the estimated mean flow. The nonlinear inviscid, SGS and source terms in the entire computational domain are then multiplied by λ. Thus, once the damping function is determined at the beginning of the simulation, the presence of the wall region is transparent computationally. There is no special procedure for the near wall region, no auxiliary wall grid and no additional complication of the parallel implementation.

The potential impact of a poorly estimated mean flow field is not addressed in this research since we consider cases in which RANS predictions are in very good agreement with experiment. It is noted, however, that there may be an impact. Flow separation may be a particular challenge for this approach (as it is with other available wall models) and will be investigated in the future. We do not anticipate any problems with using the NLD equations for separated flow in general as they have been successfully applied to unsteady laminar separated flow problems[14].

4. NUMERICAL APPROACH

4.1 Scheme

The equations outlined in sections 2 and 3 are transformed into a curvilinear coordinate system and solved using finite difference techniques. The spatial derivatives are evaluated using a sixth order central difference approximation and the solution is advanced in time using a fourth order Runge Kutta method. The unresolved, high wavenumber components of the solution are damped at each time step by adding a sixth order filter term operating on the conserved variables to the residuals. Thus, the scheme is fourth order accurate. For the boundary layer case, fourth order finite difference stencils are used at the radiation boundary opposite the wall for stability.

4.2 Parallel Implementation

The explicit algorithm described above is easily parallelized with excellent speedup using domain decomposition. At the beginning of each run, the computational domain is decomposed and distributed to the available processors. Each processor then advances the solution on its domain updating the interprocessor boundary data using the MPI library. The parallelism is transparent to the solution integration.

The results presented here have been obtained using an eight node cluster of 450 MHz Pentium III processors running the Linux operating system, a 16 node SGI Power Challenge, 16 nodes of an SGI Origin 2000 or a single 733 MHz Pentium III processor running Windows NT. The code requires, for example, $41\,\mu s$ per time step per grid point on the 733 MHz Pentium III. Details on the scalability of a very similar algorithm can be found in Morris *et al.*[1]

6

5. RESULTS AND DISCUSSION

5.1 Fully Developed Turbulent Boundary Layer

In this section, results for a fully developed turbulent boundary layer simulation without wall modeling are presented. These results serve to validate the use of the NLD equations for wall bounded flows. The efficacy of the wall model is demonstrated in the next section where turbulent channel flow results are presented.

The momentum thickness Reynolds number of the boundary layer simulated here is 5400. The Reynolds number per ft is 300,000. A freestream Mach number of 0.25 is used as a compromise between reduced compressibility effects and tolerable run time. The computational domain is $6\delta \times 3\delta \times 2\delta$ in the streamwise, wall normal and spanwise directions, respectively, where δ is the boundary layer thickness. The streamwise length given above is the distance from the inflow plane to the location where data is sampled for recycling. It does not include the buffer zone. Hyperbolic stretching is used in the wall normal direction which is discretized by 63 points. The wall spacing is set to 1^+. The streamwise and spanwise directions are discretized by 63 and 81 points, respectively. The resolution in the streamwise direction is 184^+ and 48^+ in the spanwise direction.

With this resolution, the near wall streaky structures that are spaced approximately 440^+ apart in the streamwise direction and 80^+ apart in the spanwise direction[15] will not be accurately represented by the fourth order scheme used here (for comparison, Moin and Kim[15], who used a pseudospectral method to simulate turbulent channel flow, had grid points spaced 126^+ apart in the streamwise direction and 21^+ apart in the spanwise direction.) This poorly resolved wall layer will cause some discrepancies in our comparisons, however, as will be shown, overall the results are promising. A simulation of this case with the wall model discussed in section 3.2 is currently being conducted.

Predicted mean velocity profiles are plotted in figure 1 using inner and outer coordinates and compared to the estimated solution. This solution, being determined by a RANS calculation, is considered to compare very well with experimental data for the flat plate boundary layer case (the same can be said about the turbulent channel flow case discussed in the next section).

Typical of LES of wall bounded flows using the Smagorinsky model with an underresolved wall region[16][17], the buffer region of the profile is too large and the skin friction coefficient is underpredicted (as evidenced by the high value of u^+ at the boundary layer edge). The four regions of a turbulent boundary profile, however, are clearly evident. The agreement in the sublayer is good so that a region of constant shear stress near the wall is correctly predicted. A log law region is visible with a slope close to that of the estimated mean (the y intercept is overpredicted due to the large buffer region.) A wake region is also evident and, as can be seen when plotted using outer variables, agrees quite well with the prescribed mean.

Turbulence intensity profiles are presented in figure 2. In general, the agreement with Klebanoff's experimental data is good despite the poor resolution of the near wall region. The effect of this poor resolution appears to be confined to that region. For the streamwise component, the peak is slightly overpredicted and is much smoother compared to the experimental data. This is in agreement with the overly large buffer region shown in the mean velocity profile.

The effect of the large buffer region manifests itself differently in the wall normal and spanwise intensity profiles. For the wall normal component, which does not have a strong peak near the wall, the rate at which the intensity increases is underpredicted. In contrast, the rate at which the streamwise component increases is well represented by the simulation, however, the peak evi-

7

dent in the experimental data is absent from the prediction. Beyond the buffer region, the comparison of each of the three components with the experimental data is good.

In figure 3 the predicted wall pressure power spectral density is compared to experimental data. The following inner variables are used:

$$\Phi_{pp}^+ = \frac{\Phi_{pp}(\omega)u_\tau^2}{\nu \tau_w^2}$$

$$\omega^+ = \frac{\omega \nu}{u_\tau^2}$$

(18)

For the comparisons made here, the normalization variables were calculated using the estimated mean solution.

Like the turbulence intensity profiles, the agreement with the experimental data is good, though some discrepancies are noted. One is that the decay of the spectra in the high frequency range is slightly underpredicted. In Farabee and Casarella[20], it is suggested that the structures responsible for the mid to high frequency pressure fluctuations reside in the buffer region of the boundary layer. Thus, the underpredicted decay rate of the spectra may be due to the relatively poor representation of the buffer region as discussed earlier.

The other discrepancy is that for the entire frequency range, the levels appear to be slightly overpredicted suggesting that the root mean square (RMS) of the wall pressure fluctuations is too high. Farabee and Casarella[20] compared a number of experimental measurements of the wall pressure RMS and found significant scatter. They presented a plot of the wall pressure RMS normalized by the wall shear stress as a function of the Reynolds number based on the friction velocity and boundary layer thickness. For the Reynolds number used in the present study, the normalized pressure RMS varies approximately from 2.3 to 3.5. The value predicted by the current simulation is 3.1. This happens to agree very well with the value of 3.2 given by an empirical relationship developed in Farabee and Casarella[20].

5.2 Channel Flow

In this section, preliminary results of a turbulent channel flow simulation are presented to assess the new wall model. The Reynolds number based on the centerline velocity and channel half width is 12800. Based on the friction velocity, u_τ, and channel half width the Reynolds number is 640. This corresponds to the Reynolds number used for the incompressible simulation presented by Moin and Kim[15]. For our compressible case we use a centerline Mach number of 0.10.

The computational domain is $4\pi h \times 2h \times \pi h$ in the streamwise, wall normal and spanwise directions, respectively, where h is the channel half width. Hyperbolic tangent stretching is used in the wall normal direction which is discretized by 37 points and varies from -h to h. The spacing at the walls is set to 1^+. Uniform point distributions are used in the streamwise and spanwise directions, which are discretized with 38 and 69 points, respectively. In wall units, the spacings in the streamwise and spanwise directions are 250^+ and 32^+, respectively.

The wall model results presented in this section were obtained using a Heaviside function for the variable λ defined in section 3.2. If y^+ is determined using the distance to the nearest wall, then $\lambda(y^+) = H(y_\chi^+)$. Here, we use $y_\chi^+ = 25$ which is at the inner edge of the log-law region of the estimated profile.

Predicted velocity profiles with and without the wall model are plotted in outer and inner coordinates and compared to the estimated solution in figure 4. Like the boundary layer case discussed in the previous section, the predicted velocity profile for the channel flow case has an excessively large buffer region and a wall shear stress that is too low when the wall model is not used. This simulation does, however, like the boundary layer case, predict a log-law region.

The agreement between the estimated and predicted profiles improves when the wall model is used. This is particularly true in the near wall region which is consistent with the fact that in this region the wall model forces the time mean of the perturbations to be zero. Outside of this region, however, a log-law region fails to develop and the profile in the outer region is flat compared to the estimated mean.

These shortcomings are most likely associated with the discrepancies found in figure 5 between the turbulence intensity profiles predicted here and those of Moin and Kim[15], who used a well resolved wall layer. In this figure, the intensities are normalized by the friction velocity of the estimated mean and plotted as a function of the wall normal coordinate. Only contributions to the turbulence intensity from the resolved fluctuations are considered. The unresolved contributions parameterized by the SGS model are not included. Thus, one should expect the intensities predicted here to be lower than those of Moin and Kim since they used a finer grid and resolved rather than modeled more of the turbulent energy. However, the level of disagreement cannot be completely attributed to this difference.

The wall normal and spanwise components are significantly underpredicted both with and without the wall model. In contrast, the streamwise component is overpredicted for most of the profile without the wall model and underpredicted with the wall model.

A review of the literature reveals two plausible explanations for these discrepancies. The first is associated with the wall model. Since the nonlinear terms of the governing equations are damped out in the buffer region of the boundary layer, turbulence production there, which is primarily responsible for the near wall fluctuations, is suppressed. Mason and Thompson[21] found that when a log-law type of boundary condition is used (in lieu of simulating the viscous sublayer and the buffer region) the Smagorinsky model needed to be supplemented with a stochastic backscatter model to represent the effect of the buffer region.

In contrast, Piomelli et al.[22] had good agreement between their LES turbulence intensity predictions and experimental data using a log-law approximate wall condition without a backscatter model. Their wall condition enforced the law of the wall in a spatially averaged sense while Mason and Thompson[21] enforced it locally. According to Baggett[23], this difference is responsible for success of Piomelli et al.[22] since their approach more accurately models the turbulence structural information fed into the outer region by the inner region. It should be noted that another difference between the simulations of Mason and Thompson[21] and Piomelli et al.[22] is that Mason and Thompson used a Smagorinsky model alone for the SGS stresses while Piomelli et al. used a mixed model.

SGS modeling, in fact, is the second possible explanation we consider for the discrepancies found in figure 5. As discussed in section 3.1, a constant coefficient Smagorinsky model is used here with the van Driest near wall damping to account for the variation of the turbulence length scale as the wall is approached. This type of damping may not be an optimal choice. Piomelli[24] found, in simulations of coarsely resolved high Reynolds number channel flow simulations, that the van Driest damping causes 100 times more SGS dissipation than what would be generated if the dynamic procedure for determining the Smagorinsky constant were used without the van Dri-

est damping. Thus, the dynamic Smagorinsky model will clearly increase the predicted turbulence intensity.

Based on this review, two potential improvements to our simulations are apparent. One is to incorporate a stochastic backscatter model and the other is to implement the dynamic Smagorinsky model. Piomelli's[24] finding and the success of Balaras et al.[8], who used the dynamic model with their two layer approximate wall conditions, as well as the general acceptance that the dynamic model is an improvement over the constant coefficient model, compel us to believe that it alone may be sufficient to rectify the discrepancies found in the turbulence intensity profiles.

6. CONCLUSIONS

Llarge-eddy simulations of wall bounded shear flows were conducted using the Nonlinear Disturbance Equations. Our objectives were twofold. The first was to demonstrate that these equations, which have advantages over the traditional form of the Navier Stokes equations when computational aeroacoustic problems are considered, are capable of predicting wall bounded shear flow turbulence statistics. This objective was achieved with a simulation of a flat plate boundary layer. Although the velocity profile prediction was marginal, the turbulence intensity and wall pressure spectra predictions were good.

The second objective was to build upon the advantages of using the Nonlinear Disturbance Equations by developing an efficient and easily implemented wall model. In this regard, work is not complete. The model was implemented and demonstrated some advantages. However, the turbulence intensity profiles for a channel flow simulation were significantly underpredicted. We believe that these discrepancies are associated with the decay of the subgrid-scale stresses as the wall is approached and plan to rectify the problem by implementing a more robust subgrid-scale stress model. This effort is currently underway.

REFERENCES

1. P. J. Morris, L. N. Long, A. Bangalore, and Q. Wang, A parallel three-dimensional aeroacoustics method using nonlinear disturbance equations, *J. Comput. Phys.* **133**, 56 (1997).
2. C. K. W. Tam and J. C. Webb, Dispersion-relation-preserving finite difference schemes for computational acoustics, *J. Comput. Phys.* **107**, p. 262 (1993).
3. M. B. Giles, Nonreflecting boundary conditions for Euler equation calculations, *AIAA J.* **28**(12), p. 2050 (1990)
4. J. Liu, L. N. Long, and A. Modi, Higher-order accurate solutions of ship airwake flow fields using parallel computer, presented at the *American Helicopter Society 54th Annual Forum*, Washington D. C., May 20-22, 1998.
5. J. Liu, and L. N. Long, Direct aeroacoustic and aerodynamic simulation of multi-hole engine liners, AIAA Paper 98-2330, presented at the *4th AIAA/CEAS Aeroacoustics Conf.*, Toulouse, France, June 2-4, 1998.
6. U. Schumann, Subgrid scale model for finite difference simulation of turbulent flows in plane channel and annuli, *J. Comput. Phys.* **18**, p. 376 (1975).
7. U. Piomelli, J. Ferziger, P. Moin, and J. Kim, New approximate boundary conditions for large eddy simulations of wall bounded flows, *Phys. Fluids A* **1**, p. 1061 (1989).
8. E. Balaras, C. Benocci, and U. Piomelli, Two-layer approximate boundary conditions for large-eddy simulations, *AIAA J.* **34**(6), p. 1111 (1996).
9. C. G. Speziale, Turbulence modeling for time-dependent RANS and VLES: a review, *AIAA J.* **36**(2), p. 173 (1998).

10. L. J. Peltier, F. J. Zajaczkowski, and J. C. Wyngaard, A hybrid RANS/LES approach to large-eddy simulation of high-Reynolds-number wall-bounded turbulence, in *Proc. of ASME FEDSM'00*, FEDSM2000-11177 (2000).
11. T.S. Lund, X. Wu, and K.D. Squires, Generation of turbulent inflow data for spatially-developing boundary layer simulations, *J. Comput. Phys.* **140**, p. 233 (1998).
12. B. Wasistho, B. J. Geurts, and J. G. M. Kuerten, Simulation techniques for spatially evolving instabilities in compressible flow over a flat plate, *Computers & Fluids* **26**, p. 713 (1997).
13. P. Moin, K. Squires, W. Cabot, and S. Lee, A dynamic subgrid-scale model for compressible turbulence and scalar transport, *Phys. Fluids A* **3**, p. 2746 (1991).J.
14. R. Hansen, and L. N. Long, Steady and unsteady laminar flow simulations using the Nonlinear Disturbance Equations, AIAA Paper 2000-2330, presented at the *6th AIAA/CEAS Aeroacoustics Conf.*, Lahaina, Hawaii, June 12-14, 2000.
15. P. Moin, and J. Kim, Numerical investigation of turbulent channel flow, *J. Fluid Mech.* **118**, p. 341 (1982).
16. E. T. Spyropoulos, and G. A. Blaisdell, Large-eddy simulation of a spatially evolving supersonic turbulent boundary-layer flow, *AIAA J.*, **36**(11), p. 1983 (1998)
17. A. Pascarelli, U. Piomelli, and G. V. Candler, Multi-block large-eddy simulations of turbulent boundary layers, *J. Comput. Phys.*, **157**, p. 256 (2000).
18. H. Schlichting, *Boundary-Layer Theory* (McGraw-Hill, New York, 1987), p. 567.
19. S. P. Gravante, A. M. Naguib, C. E. Wark, and H. M. Nagib, Characterization of the pressure fluctuations under a fully developed turbulent boundary layer, *AIAA J.*, 36(10), p. 1808 (1998).
20. T. M. Farabee, and M. J. Casarella, Spectral features of wall pressure fluctuations beneath turbulent boundary layers, *Phys. Fluids A* **3**, p. 2410 (1991).
21. P. J. Mason, and D. J. Thompson, Stochastic backscatter in large-eddy simulations of boundary layers, J. Fluid Mech. 242, p. 51 (1992).
22. U. Piomelli, J. Ferziger, P. Moin, and J. Kim, New approximate boundary conditions for large eddy simulations of wall-bounded flows, *Phys. Fluids A* 1, p. 1061 (1989).
23. J. S. Baggett, Some modeling requirements for wall models in large eddy simulation, *Annual Research Briefs 1997* (Center for Turbulence Research, Stanford University, Stanford, CA), p. 123 (1997).
24. U. Piomelli, High Reynolds number calculations using the dynamic subgrid-scale stress model, *Phys. Fluids A* **5**, p. 1484 (1993).
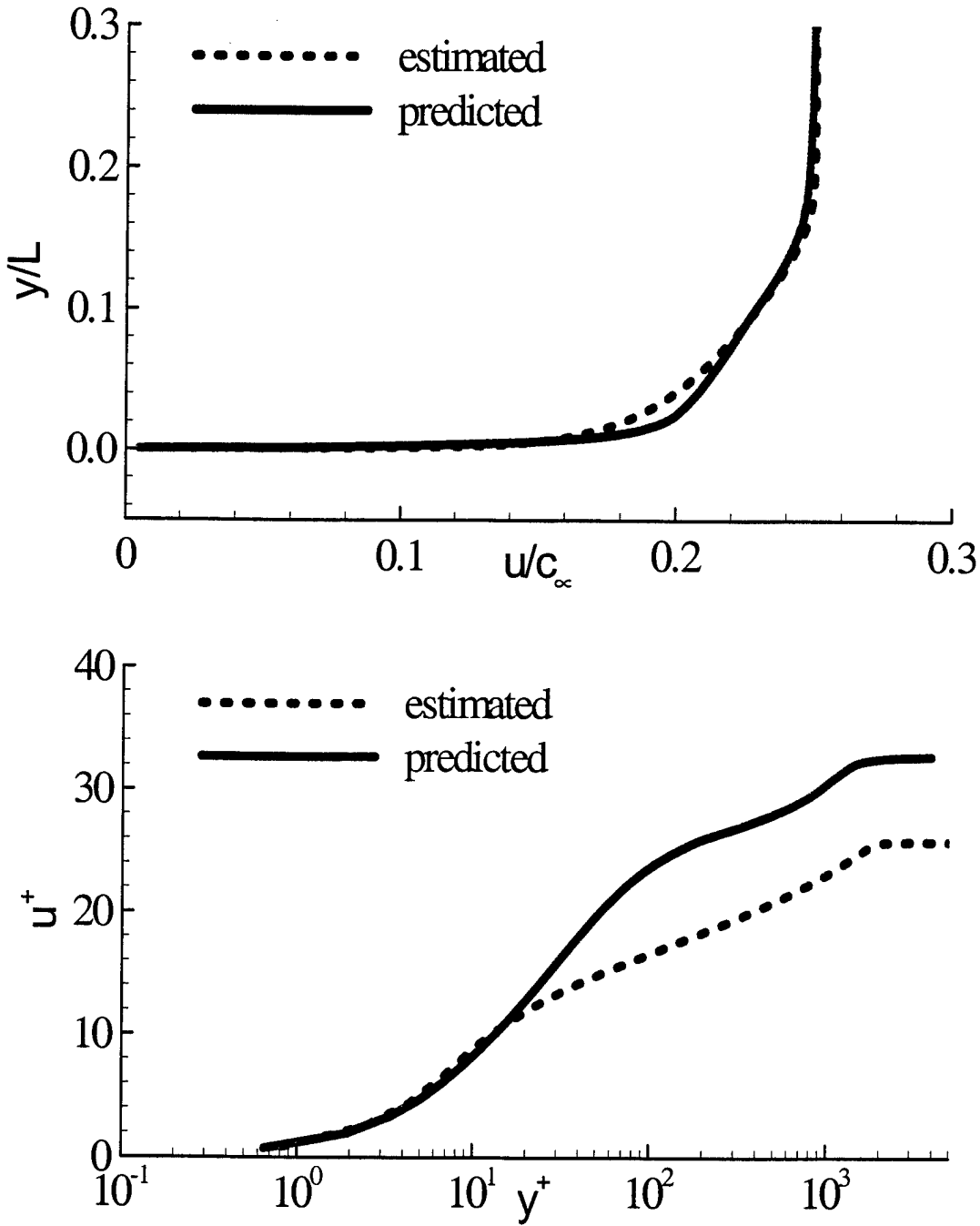
FIG. 1. Predicted mean velocity profiles for the fully developed turbulent boundary layer case plotted on outer (top) and inner (bottom) coordinates compared to the prescribed solution.
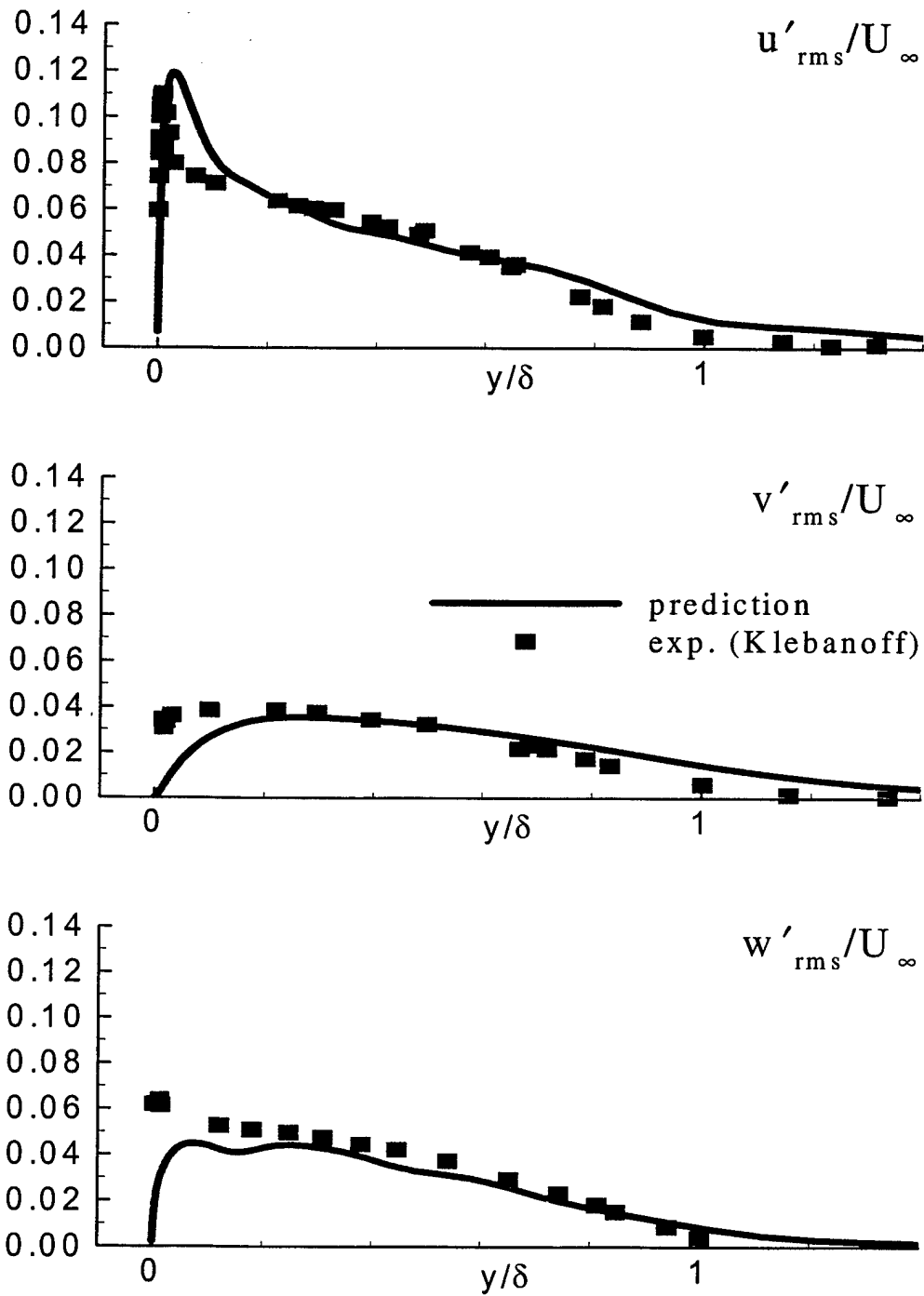
FIG. 2. Predicted turbulence intensity profiles for the fully developed turbulent boundary layer cas compared to experimental data (taken from Schlichting[18]). Top - streamwise, middle - wall noi nal, bottom - spanwise.
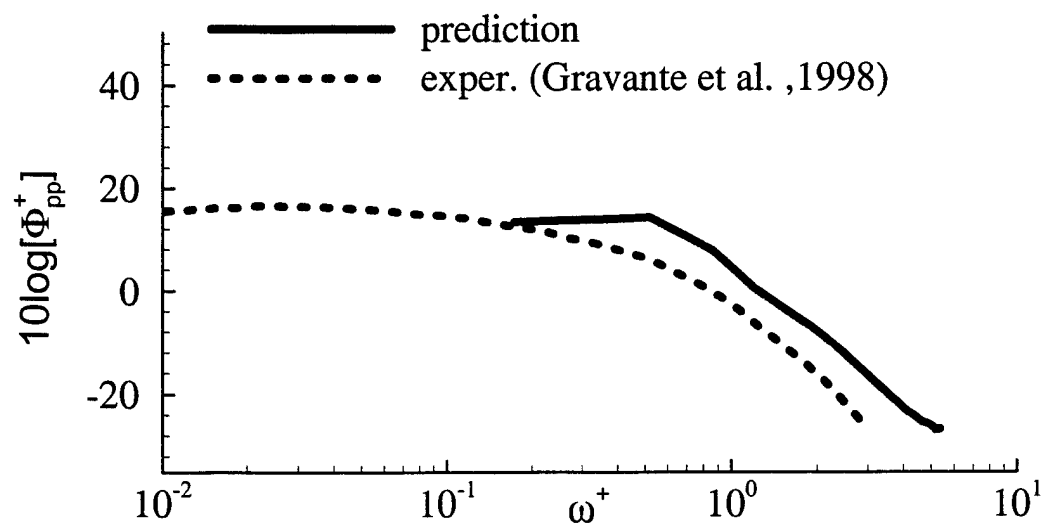
FIG. 3. Predicted fully developed turbulent boundary layer wall pressure power spectral density normalized by inner coordinates compared to experimental data taken from [19].
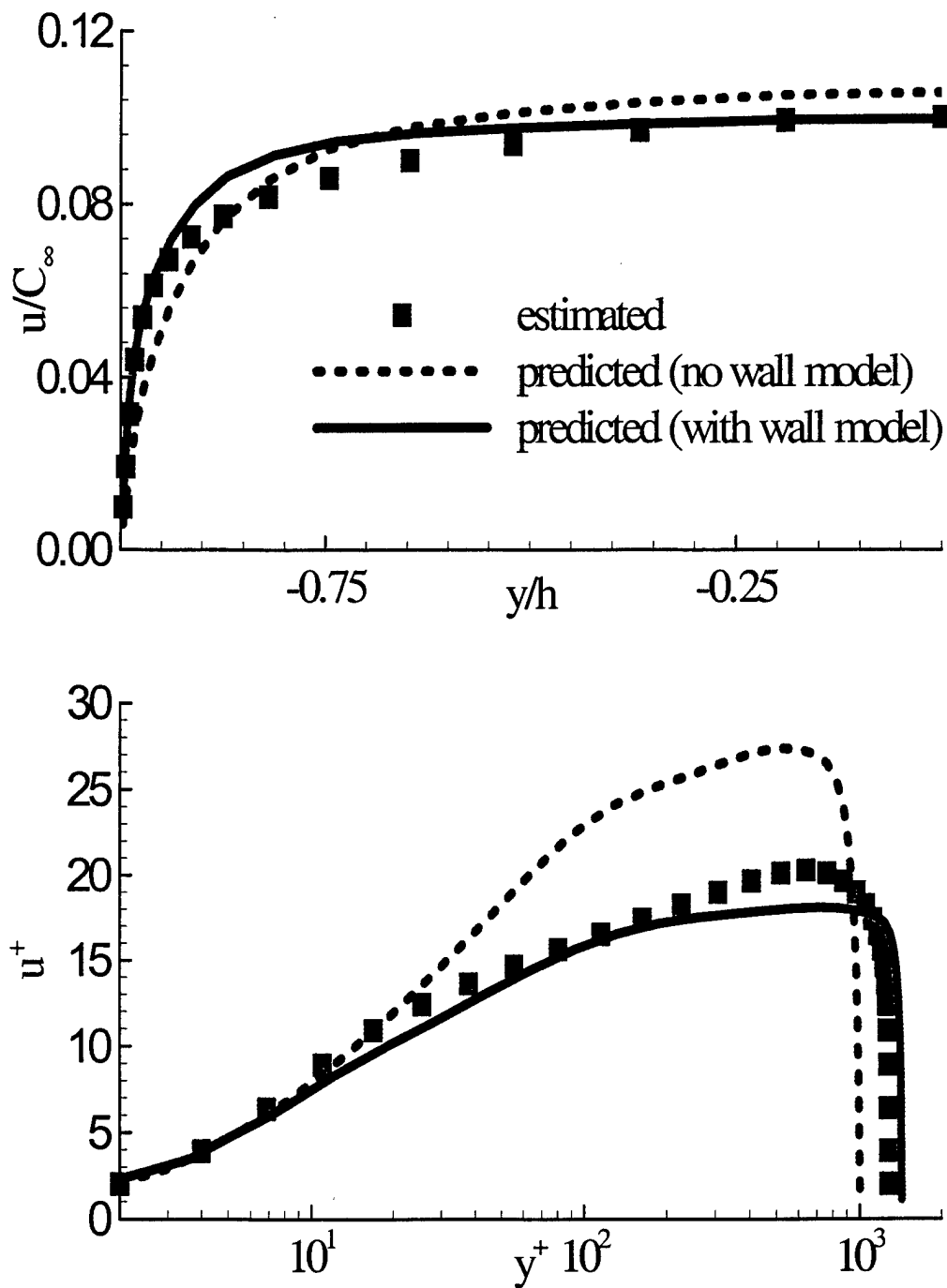
FIG. 4. Predicted
mean velocity profiles for the turbulent channel flow case plotted in outer (top) and inner (bottom) coordinates compared to the estimated mean solution.
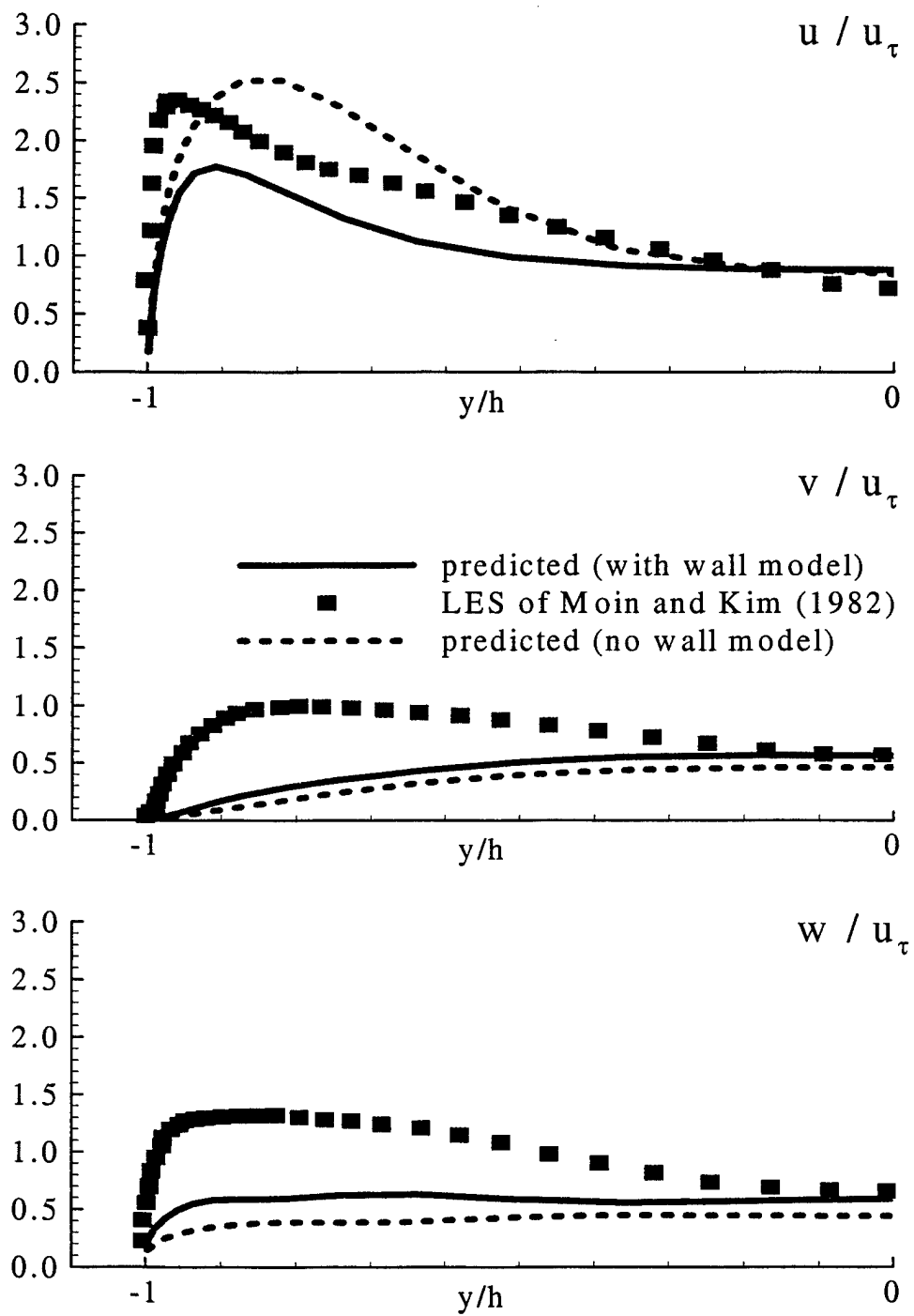
FIG. 5. Predicted turbulence intensity profiles for the turbulent channel flow case. Top - strea wise, middle - wall normal, bottom - spanwise.

REPORT DOCUMENTATION PAGE

Public reporting burden for this collection of information is estimated to average 1 hour per response, including the time for reviewing instructions, searching existing data sources, gathering and maintaining the data needed, and completing and reviewing the collection of information. Send comments regarding this burden estimate or any other aspect of this collection of information, including suggestions for reducing this burden, to Washington Headquarters Services, Directorate for Information Operations and Reports, 1215 Jefferson Davis Highway, Suite 1204, Arlington, VA 22202-4302, and to the Office of Management and Budget, Paperwork Reduction Project (0704-0188), Washington, DC 20503.

1. AGENCY USE ONLY (Leave Blank)	2. REPORT DATE 7/11/00	3. REPORT TYPE AND DATES COVERED Final

4. TITLE AND SUBTITLE
Trailing Edge Noise Prediction
Large-Eddy Simulation of Wall Bounded Shear Flow Using the Nonlinear Disturburbance Equations

5. FUNDING NUMBERS
N-00014-99-0290

6. AUTHORS
Thomas S. Chyczewski, ARL Penn State
Philip J. Morris, Dept. Aerospace Engineering
Lyle N. Long, Dept. Aerospace Engineering

7. PERFORMING ORGANIZATION NAME(S) AND ADDRESS(ES)
Applied Research Laboratory
The Penn State University
Post Office Box 30
State College, PA 16804

8. PERFORMING ORGANIZATION REPORT NUMBER

9. SPONSORING / MONITORING AGENCY NAME(S) AND ADDRESS(ES)
Dr. L. Patrick Purtell
Office of Naval Researchq
800 North Quincy St.
Arlington, VA 22217-5660

10. SPONSORING / MONITORING AGENCY REPORT NUMBER

11. SUPPLEMENTARY NOTES

12a. DISTRIBUTION / AVAILABILITY STATEMENT
Unlimited

12b. DISTRIBUTION CODE

13. ABSTRACT (Maximum 200 words)

The potential benefits of using the Nonlinear Disturbance (NLD) equations, which govern flow variable fluctuations about an estimated mean, for the large-eddy simulation (LES) of wall bounded shear flows are investigated in this paper. In addition to verifying the suitability of the NLD equations for wall bounded flows, we build upon its advantages by introducing a new wall model that is easily and efficiently implemented within the NLD equation framework. The model implementation consists of defining a near wall region in which a modified linear set of equations are solved. The linear equation set allows disturbances to pass through and interact with the wall without altering the estimated mean. The streamwise and spanwise grid resolution of this near wall region can therefore be significantly relaxed while maintaining reasonable mean quantities such as skin friction. Comparisions of predicted turbulence intensity profiles and wall pressure spectra to experimental data for a fully developed turbulent flat plate boundary layer are used to verify the suitability of the NLD equations for wall bounded flows. Preliminary results of a turbulent channel flow simulation are also presented to assess the new wall model.

14. SUBJECT TERMS

15. NUMBER OF PAGES

16. PRICE CODE

17. SECURITY CLASSIFICATION OF REPORT UNCLASSIFIED	18. SECURITY CLASSIFICATION OF THIS PAGE UNCLASSIFIED	19. SECURITY CLASSIFICATION OF ABSTRACT UNCLASSIFIED	20. LIMITATION OF ABSTRACT SAR